Nuclear Science and Techniques (2023) 34:103
https://doi.org/10.1007/s41365-023-01255-7

Development of short prototype of dual aperture quadrupole magnet for CEPC ring

Mei Yang[1,2,3] · Fu-San Chen[1,2,3] · Ya-Feng Wu[1,2] · Zhuo Zhang[1,2] · Bao-Gui Yin[1,2] · Bin Na[4] · Zhan-Jun Zhang[4]

Received: 12 February 2023 / Revised: 6 April 2023 / Accepted: 26 April 2023 / Published online: 17 July 2023

Abstract
Main quadrupole magnets are critical for the Circular Electron and Positron Collider (CEPC) and are specifically designed as dual aperture quadrupole (DAQ) magnets. However, the field crosstalk between the two apertures presents challenges. As the CEPC will work at four beam energies of Z, W, Higgs and ttbar mode, the DAQ magnets will operate at four field gradients spanning from 3.18 to 12.63 T/m. The first short quadrupole magnet prototype with the bore diameter of 76 mm and magnetic length of 1.0 m revealed the problems of large magnetic field harmonics and a magnetic center shift within the beam energy range. Accordingly, a compensation method was proposed in this work to solve the field crosstalk effect. By adjusting the gap height at the middle of the two apertures, the field harmonics and magnetic center shift are significantly reduced. After optimization, the short prototype was modified using a new scheme. The field simulations are validated from the magnetic measurement results. Further, the multipole field meets the requirements of the four beam energies. The detailed magnetic field optimization, field harmonics adjustment, and measurement results are presented herein.

Keywords Dual aperture magnets · Field measurements · Crosstalk effect · Quadrupole magnet · Field harmonics · CEPC

1 Introduction

The Circular Electron Positron Collider (CEPC) is a machine that has been proposed for construction in China, mainly as a Higgs factory. Its circumference is approximately 100 km, and its collider has a double-ring lattice. More than 80 km of the CEPC tunnel is covered with magnets. Because the individual magnetic fields are low, most are designed as iron-dominated magnets, which are economical and effective for shaping the field. The two rings require a large number of dipole, quadrupole, sextupole, and corrector magnets [1–4]. The obtained magnets were sorted and grouped into small batches. Unlike a general collider with single aperture quadrupole magnets [5–7], the double-ring collider has a similar length and strength or gradient for dipole and quadrupole magnets, so a dual aperture magnet scheme similar to that proposed by FCC-ee [8–10] is adopted to reduce the magnet number and power consumption, resulting in savings of approximately 50% of the power consumption compared with that for two separate magnets.

Table 1 lists the main specifications of the dual aperture quadrupole (DAQ) magnets. The collider works in the Z, W, Higgs, and ttbar modes, corresponding to beam energies of 45.5, 80, 120, and 180 GeV, respectively. For different working modes, except the radio frequency (RF) region, compatible lattices were obtained following scaling down of the magnetic strength with energy. The magnets cover the four different energies and exhibit a large dynamic range. The collider ring comprises only two RF cavities [11, 12], and significant synchrotron radiation exists along the ring; therefore, a corresponding energy sawtooth effect occurs [13, 14]. To compensate for this, the trim coils are added in the main dipole and quadrupole magnets. The individually trim coils in each aperture influence the field strength or

✉ Mei Yang
yangmei@ihep.ac.cn

1 Institute of High Energy Physics, Chinese Academy of Sciences, Beijing 10049, China

2 Key Laboratory of Particle Acceleration Physics and Technology, Institute of High Energy Physics, Chinese Academy of Sciences, Beijing 100049, China

3 University of Chinese Academy of Sciences, Beijing 100049, China

4 Beijing HE-Racing Technology Co., Ltd., Beijing 1000049, China

Table 1 Basic requirements of CEPC dual aperture quadrupole (DAQ)

Item	Value
Aperture diameter (mm)	76
Field gradient, 45.5 GeV ~ 180 GeV (T/m)	3.18–12.63
Magnetic length (mm)	2000
Reference radius (mm)	12.2
Multipole field content (1×10^{-4})	≤ 5
Adjustment ability	$\leq 1.5\%$
Central field difference	$\leq 0.5\%$

gradient in one aperture without affecting the magnetic field quality of the other aperture. The trim coils were gradually adjusted at different positions on the ring relative to the distance from the RF station. In addition, these trim coils can handle the dispersion of the magnetic field strength between the magnets.

The DAQ magnet has opposite polarities in two apertures: one focused and the other defocused. Further, this magnet shares two pancake coils that excite two apertures, instead of eight as for two separate quadrupole magnets [15, 16]. Because of these special requirements, the design of a DAQ magnet is not without technical challenges: The key issue is the magnetic crosstalk between the two apertures. The installation of shared coils results in division of the yoke into several parts, adding to the mechanical complexity. Thus, magnetic design, mechanical design, fabrication cost, and power consumption should be carefully considered.

The preliminary design and field measurement results of a 1-m-short DAQ magnet prototype are summarized in Sect. 2. The magnetic optimization is described in Sect. 3. A novel scheme involving center shim adjustment to balance the flux line distributions in individual apertures of the DAQ magnet is proposed. Different trim coil layout schemes are compared, and an optimized scheme is selected. Section 4 briefly introduces a modification of the short prototype. Section 5 describes the magnetic center shift adjustment in the horizontal direction. In addition, the principle of harmonic adjustment using a magic finger is briefly reviewed, and the final adjustment scheme is presented along with the field measurement results. Finally, the conclusions are provided in Sect. 6.

2 Preliminary design and field measurement of short DAQ magnet prototype

The distance between the electron and positron beams in the collider of CEPC is 350 mm, determined by the excitation coil, vacuum chamber, cooling tube, and lead block in the

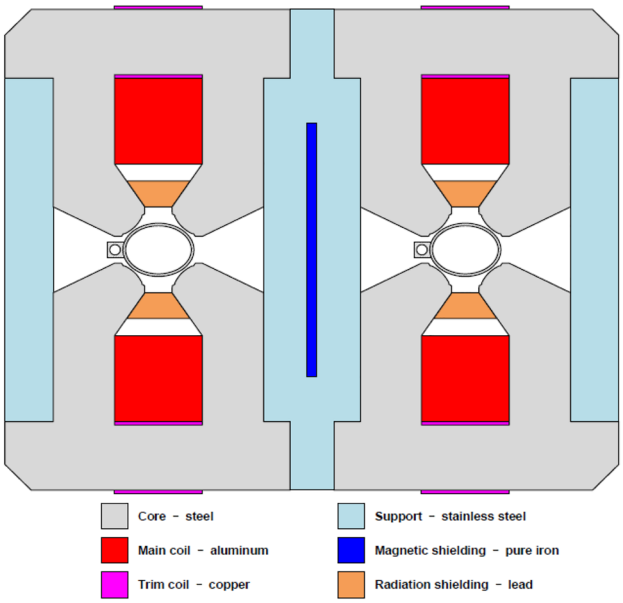

Fig. 1 (Color online) Preliminary cross section of first dual aperture quadrupole (DAQ) magnet prototype

dual aperture dipole magnet. Field gradients for the quadrupole magnet range from 3.18 to 12.63 T/m. The maximum pole–tip magnetic field is 0.48 T at 180 GeV.

Because there are approximately 2000 quadrupole magnets in the CEPC with the length of 2 m, several aspects were considered to reduce the respective construction costs and power consumption. A laminated prototype was selected for magnet consistency and ease of processing. Hollow aluminum conductors are used for exciting coils to reduce cost and weight. A low current density and high voltage were chosen to reduce the power loss in the magnet and cables connecting the magnet to the power supply. The preliminary cross section of the 1-m-short DAQ magnet prototype is shown in Fig. 1. The iron is divided into several pieces for coil installation [17]. To reduce the magnetic coupling effects, a 50 mm stainless steel plate with a DT4 sheet inserted in between was used to decouple the two apertures. Trim coils were wound on the top and bottom yokes. Yellow lead blocks (Fig. 1) were placed between the poles to protect the exciting coil from synchrotron radiation.

The first short quadrupole magnet prototype was fabricated with the bore diameter of 76 mm and length of 1.0 m in 2019. Magnetic field simulations of the DAQ magnet were performed using the electromagnetic software OPERA [18]. The 2D simulation in the Higgs mode demonstrated that with an increase in the thickness of the DT4 sheet, b_1 and b_3 in one aperture increase, and the change ratio of b_1 to b_3 is fixed and unidirectional. Using an appropriate thickness of the DT4 sheet, b_1 and b_3 can be reduced. Preliminary field measurements were performed

using a Hall probe measurement system (Fig. 2). The results indicate that the leakage field is large and extended. As the current increases from 58 to 234 A, the magnetic center shifts, corresponding to the beam energy from 45.5 to 180 GeV. The overall offset of the magnetic center in the horizontal direction (X-axis) is approximately 1.7 and 2 mm in the two apertures, which is unacceptable for accelerator physics. This is due to the field crosstalk effect between the two apertures. When the excitation current increased, the DT4 sheet in the middle quickly saturated and the compensation capability was insufficient. In addition, the magnetic field is heavily influenced by the trim coils, which exacerbates the change in the magnetic center. Further, magnetic field simulations showed that in the preliminary design, compensation using the DT4 sheet was optimized only in the Higgs mode. In other working modes, the harmonics of the magnetic field in the two apertures cannot satisfy the design requirements. Therefore, the short DAQ magnet prototype requires further optimization and modification.

In this paper, a_n and b_n are the $2n$-th skew and normal multipole components normalized to the main quadrupole magnetic field in units of 10^{-4} at the reference radius of 12.2 mm in CEPC quadrupole magnets.

The first quadrupole magnet prototype in the FCC-ee exhibits similar problems. In the energy range of 45.5–180 GeV, the measured magnetic center shift in the horizontal direction is approximately 0.4 mm, and the sextupole field component is as large as 57 units in each aperture [19].

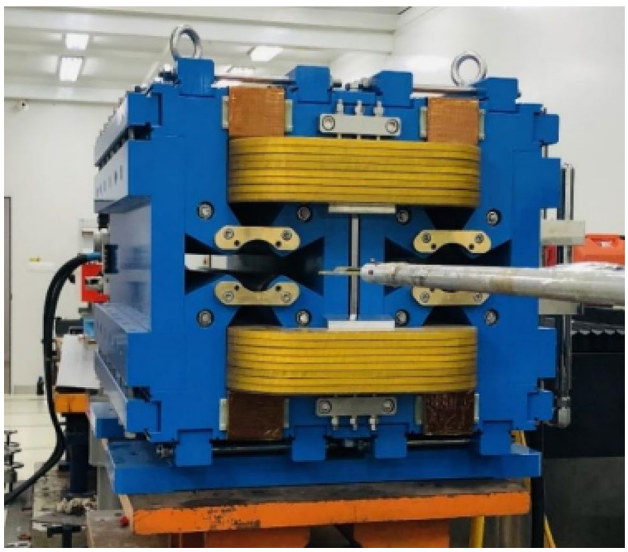

Fig. 2 (Color online) First short DAQ magnet prototype on a Hall probe measurement system

3 Optimization of DAQ magnet

In a normally conducting quadrupole magnet, the field quality mainly depends on the pole profile and symmetry of the iron yoke [20, 21]. Moreover, such quadrupole magnets usually exhibit four-fold symmetry, whereas the CEPC DAQ magnet is a type II quadrupole magnet presenting figure-of-eight. Constrained by the shared coils, the DAQ magnet has opposite polarities in the two apertures and the outer yoke should be opened in the midplane, similar to a Collins quadrupole magnet [22]. As the two apertures share one coil, they exhibit intrinsic magnetic coupling, which mainly affects the dipole and sextupole fields of both apertures.

As discussed in this section, three key aspects were considered in the re-optimization of the DAQ magnet. The first was to compensate for field crosstalk effects, which reduce the magnetic center in the horizontal direction and its shift within the energy range. The second was to minimize higher-order field harmonics. Third, the trim coil was placed at a suitable position to ensure that only the field gradient in its aperture was adjusted and that no additional field harmonics were generated in the two apertures.

3.1 Optimization of quadrupole magnetic field in 2D

Various attempts have been made to compensate for field crosstalk effects. The first involved expanding the beam separation from 350 to 500 mm. The dipole field components were reduced from 2359 to 1624 units, which was far from the requirement. However, this approach does not completely resolve the problem. Simultaneously, the volume of the magnet directly increases, and hence, the power consumption increases.

The second attempt involved adding local shims inside or outside the pole tip; however, this does not work and affects the field in the other aperture. Thus, local shim cannot resolve crosstalk effects between the two apertures.

The magnetic pole profile and yoke symmetry determine the magnetic field quality of a multipole magnet. Unlike ordinary quadrupole magnets with four-fold symmetry, the single aperture of the DAQ magnet has only up-and-down symmetry in its cross section. First, owing to the shared coil, the structures of the left and right apertures were balanced and symmetrical. Second, for a single aperture, the left and right sides of the yoke are asymmetrical because of the presence of an iron core in another aperture. Therefore, for a single aperture, this asymmetry must be counteracted through asymmetric shimming so that the magnetic flux distribution is symmetrical. This is the basic principle of compensation.

Two options were considered for modifying the DAQ magnet. The first was an entire upper or lower core for the two apertures, and the second was two separate cores for each aperture, as shown in Fig. 3. The optimization scheme uses a center shim at the horizontal gap to guarantee the symmetry of the left and right apertures, as depicted in Fig. 4. The magnetic properties of each aperture of the DAQ magnet became symmetric when the middle of the yoke protruded.

Because the shared main coils have properties similar to those of the dipole coils, a large dipole field is generated. Meanwhile, sextupole field b_3 is systematic high-order dipole field b_1; therefore, b_3 and b_1 are strongly correlated. In the 2D model, the change in b_3 was linearly proportional to that in b_1, with a ratio of approximately 0.08, which was used to estimate the center shim size. After several iterations, the optimized center shim size is 70 mm in width and 19.8 mm in height, and the final multipole components are − 0.5 units for b_1 and − 0.06 units for b_3, respectively.

The second scheme involves decoupling the iron as two yokes separated with a gap. Figure 3b presents the modified cross section of the DAQ magnet with separate iron cores, and the flux distribution in each aperture is symmetric. The gap between the two iron yokes is 80 mm, and the central yokes are wider than the outer yokes. Considering the mechanical properties and saturation, different yoke gaps can be optimized independently.

In the numerical simulations, both schemes met the same field specifications as the DAQ magnet. The entire yoke scheme has a more stable mechanical structure and lower magnetic saturation. The structure of the core is significantly simplified if a U-shaped copper-plate coil that can be inserted from one end of the magnet is used [23]. The entire iron core comprises two pieces of lamination: upper and lower halves. This facilitates the mass production of magnets. Meanwhile, in the separated yoke scheme, iron saturation is slightly higher, particularly at the highest energy. The mechanical complexity is also higher, and there are more sources of error. Therefore, the entire iron yoke scheme was used for reconstruction of the DAQ magnet and selected as the baseline of the DAQ magnet. A separated iron core scheme was selected as an alternative.

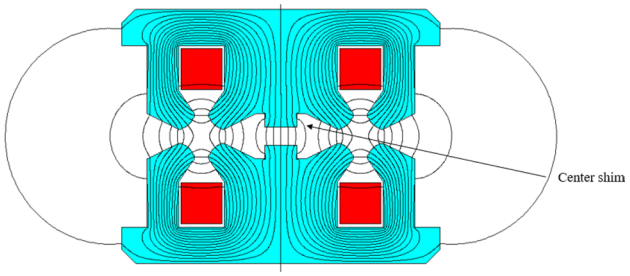

Fig. 4 (Color online) Optimized DAQ magnet with center shim

3.2 Layouts of trim coils

Because many arc quadrupole magnets with the same gradient are distributed throughout such a long collider, it is not economical to excite every magnet using a separate power supply. Thus, several quadrupole magnets are powered in series. These magnets have integral field gradient dispersion. Furthermore, only two RF stations are present in the ring, and the synchrotron radiation is very large; therefore, there is a large-energy sawtooth effect along the ring, particularly at high energies. Coils were trimmed accordingly, compensating for the sawtooth effect and magnet dispersion in the ring. The maximum field gradient tunability of the trim coils is ± 1.5%.

In an iron-dominated magnet, the field quality is determined primarily via the pole profile and assembly accuracy of the magnet. And the magnetic circuit is determined by the magnetic length, iron core layout and the location of the excitation source.

Three trim coil layouts were analyzed for the DAQ magnet in the 2D simulations, as illustrated in Fig. 5. In the first configuration, the trim coils were wound on the top and bottom of the return yokes; the second configuration for the trim coils was on the pole root region, and the third was in the pole tip region. The first two layouts contained twice the number of turns as the third layout, with four coils in each aperture.

The central region of the aperture produces strong synchrotron radiation, through which the beam passes. However, the excitation coils contain materials for insulation

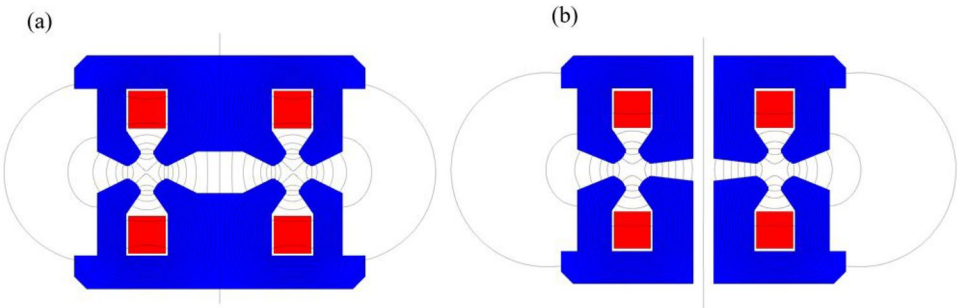

Fig. 3 (Color online) **a** Entire iron yoke scheme, and **b** separated yoke scheme

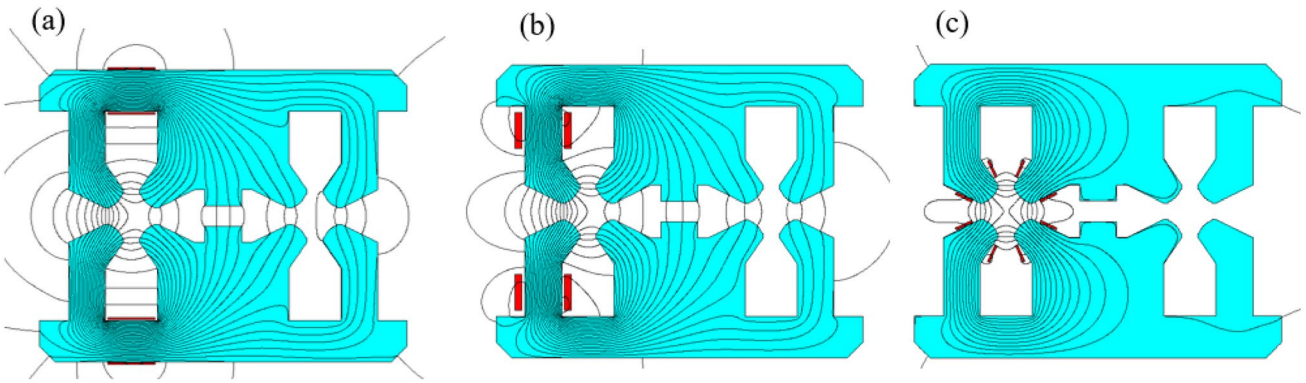

Fig. 5 (Color online) Flux line distribution in the DAQ magnet for three trim coil configurations. Only the trim coils are excited. **a** Trim coils on top/bottom of yoke; **b** Trim coils wound on left arm; **c** Trim coils wound on poles

that is not resistant to this radiation. Therefore, the exciting coils should be placed as far away from this area as possible. The first option for the trim coils involves winding of the top and bottom yokes. Magnetic field simulations were performed for these three configurations, and the corresponding flux lines are plotted in Fig. 5. When only the correction coil of the left aperture is excited, flux lines appear in the right aperture, indicating that the trimming coil affects the field in the right aperture and creates a dipole field, as shown in Fig. 5a. In Fig. 5b, the trimmer coil is on the left arm, and the flux lines penetrate the right aperture. Owing to the very high magnetic permeability of iron compared with the air region, the reluctance in iron is much smaller than that of the air in the central gap, and the flux lines are dispersed in the two apertures. However, as depicted in Fig. 5c, the magnetic circuit loop is almost closed in one aperture.

In the separated iron yoke scheme, when the trim coils are wound on the top and bottom yokes, there are fewer flux lines in the right aperture, and the main field is a dipole field, as can be seen in Fig. 6a. This is because the gap between the two yokes introduced a large magnetic reluctance. However, there is still an extra dipole field in the other apertures. Further, as shown in Fig. 6b, this was almost the same as that depicted in Fig. 5c.

The optimal location for the trim coils was wound on the four poles, displaying little effect on the field quality in the other aperture. Independent correction power supplies were used for the two apertures. This configuration produces the same flux distribution in the four poles as normal quadrupole magnetic coils. In Figs. 5c and 6b, nearly no flux lines appear in the other apertures, which exhibit the best performance for magnetic gradient fine-tuning. An evident disadvantage of this configuration is the proximity of the coils to the aperture region with large synchrotron radiation. All the trim coils require shielding protection.

3.3 3D optimization for DAQ magnet

A 3D simulation was performed to obtain the longitudinal dependence of the fundamental and higher-harmonic contents. Typically, in long magnets, the magnetic field in the midplane of a 3D model is consistent with that in a 2D model. In the DAQ magnet, unlike standard quadrupole magnet coils, the shared main coil produces an extended dipole field with significant effects at the quadrupole magnet

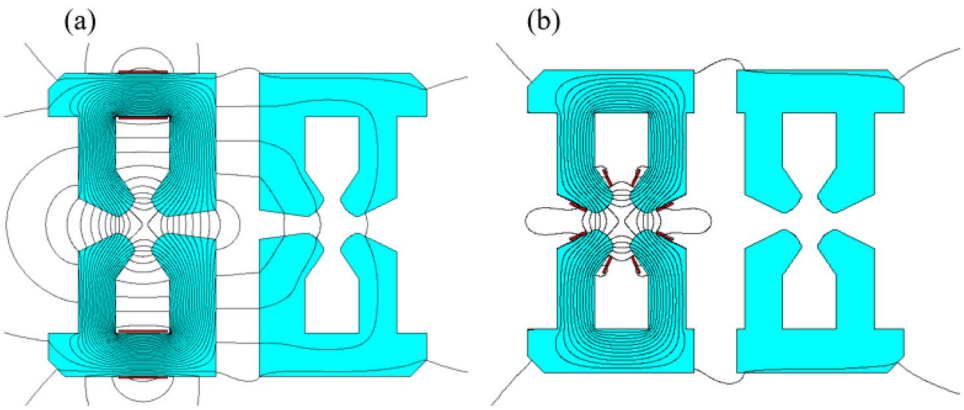

Fig. 6 (Color online) Flux line distribution in separated iron DAQ magnet for different trim coil configurations. Only trim coils are excited. **a** Trim coils wound on top/bottom of yoke; **b** Trim coils wound on poles

ends. Furthermore, in this Collins-type quadrupole magnet, fringe fields exist not only at the longitudinal ends, but also at the horizontal opening side. The field harmonics in the 3D model differ from those in the 2D simulation. When the iron length is the same, the effective length of the dipole magnet is greater than that of the quadrupole magnet [24], and hence, the dipole field should be reconsidered in the 3D simulation. In addition, the shim size should be reoptimized based on 3D simulation results. Accelerator physics requires the three-dimensional integrated magnetic field quality of a quadrupole magnet.

The developed short prototype was optimized based on the entire iron yoke scheme, and the final 3D model is depicted in Fig. 7. The resulting center shim size was 70 mm in width × 41 mm in height, which is not the same as that in the 2D simulation.

As shown in Fig. 8, the distribution of the quadrupole magnetic field is standard; however, the dipole field rises steeply and persists for a long distance. The DAQ magnet had an effective length of 1.053 m. Table 2 lists the calculated integrated multipole components of the DAQ magnet at different energies. The change in the b_3 component is less than one unit, and the multipole fields at different energies are smaller than five units, meeting the corresponding requirements. The magnetic center on the X-axis varied by 0.015 mm in the specified energy range. The trim coils wound on the poles had little effect on the multipole fields.

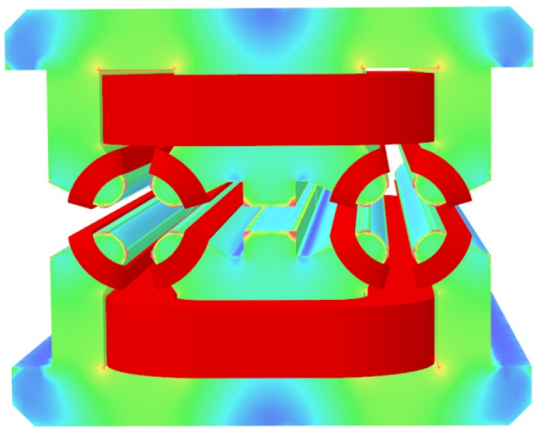

Fig. 7 (Color online) 3D magnetic simulation model of DAQ magnet with trim coils wound on poles

Table 2 Multipole field in right aperture of DAQ at different energies ($\times 10^{-4}$)

n	b_n_45.5 GeV	b_n_120 GeV	b_n_180 GeV
3	− 1.76	− 1.77	− 2.31
4	0.57	0.61	0.63
5	0.03	0.03	0.03
6	− 1.05	− 1.06	− 1.07

4 Modification of DAQ magnet prototype and mechanical measurement

The prototype was modified based on a 3D simulation of a DAQ magnet. The center stainless steel spacer was replaced with soft iron DT4 with a center shim. A schematic of this process is provided in Fig. 9. The other parts of the magnet were maintained constantly. The DAQ magnet comprises two main coils, each with 64 turns. The conductor is composed of a hollow square aluminum wire with the side length of 11 mm and a cooling hole with the diameter of 7 mm. The operating currents were 50, 154, and 234 A, corresponding to energies of 45.5, 120, and 180 GeV, respectively.

To install the soft iron DT4 with a center shim, the DAQ magnet must be disassembled. Because the mechanical structure was not as strong as possible, the precision of the reassembly was poor. The mechanical measurement results in the magnet pole end region are presented in Fig. 10, and

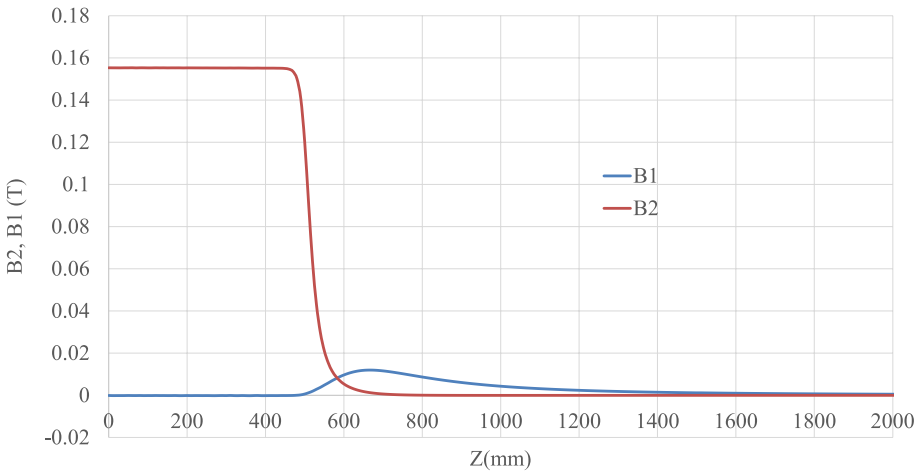

Fig. 8 (Color online) Distribution of dipole and quadrupole magnetic fields along Z axis @ 180 GeV

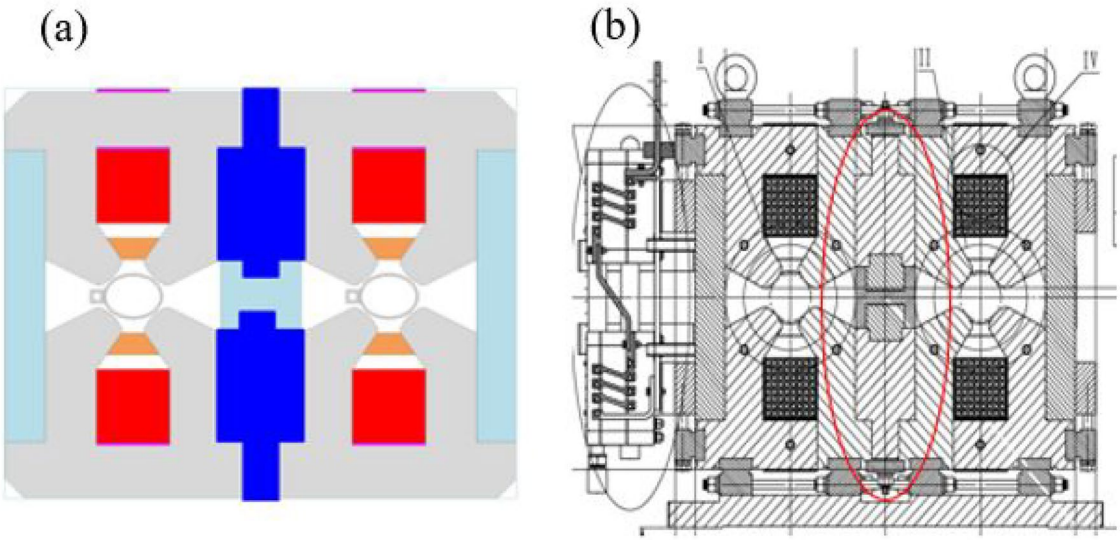

Fig. 9 (Color online) Schematic model and drawings of modified DAQ magnet. Dark blue areas indicate DT4 material. Left aperture is aperture A, the right aperture is aperture B

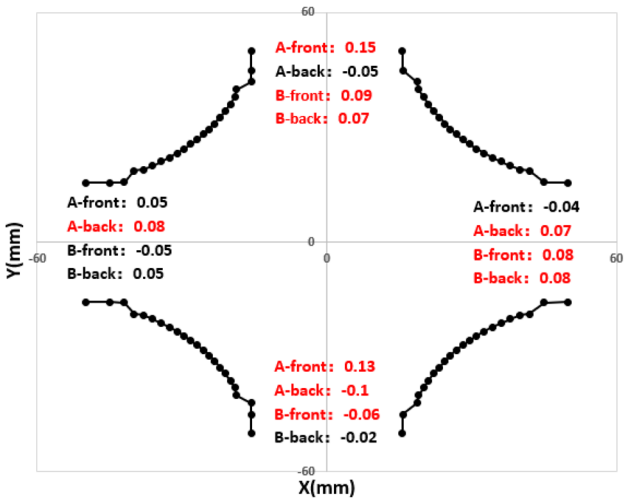

Fig. 10 Adjacent pole gap tolerance of modified DAQ magnet

most of the gaps between the adjacent poles are significantly out of tolerance. In this DAQ magnet, the aperture closest to the busbars is defined as aperture A and the other as aperture B.

5 Field measurement and improvement

5.1 First field measurement

The modified DAQ magnet was examined using a high-precision rotating coil measurement system based on a CMM [25]. A new rotating coil was fabricated via a

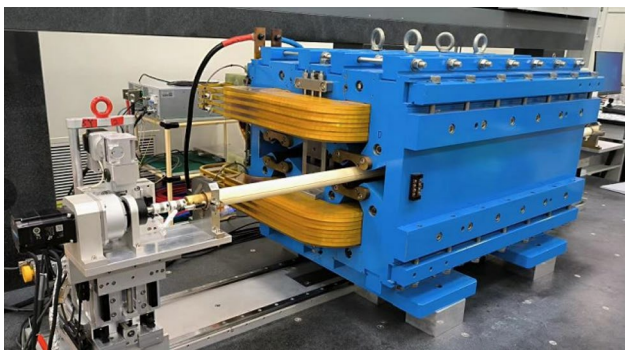

Fig. 11 (Color online) Modified DAQ magnet prototype placed on rotating coil measuring bench

compensation coil scheme [26–30] that bucks out the dipole and quadrupole magnet terms and increases the system sensitivity to high-order field harmonics. The framework of the coil was a ceramic made of Al_2O_3, which has good mechanical stiffness and hardness. The shaft has an outer radius of 20 mm and the length of 1.9 m, covering the entire range of magnetic field regions. Figure 11 shows the modified DAQ magnet prototype mounted on a rotating coil measurement bench.

After three standardization cycles with current ramping from 0 to 234 to 0 A, field measurements were carried out. The integral transfer functions of the two apertures are displayed in Fig. 12. The curve shows that the excitation efficiency was approximately 97% at 234 A, and the iron was not significantly saturated. The transfer functions in the two apertures are very similar, and the maximum difference is approximately 0.2% at the low current of 20 A.

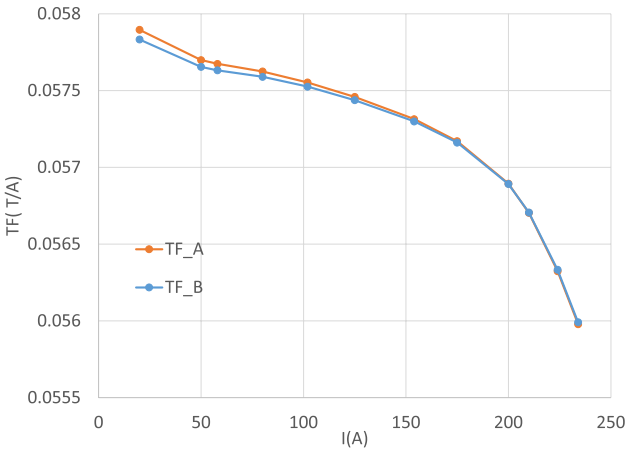

Fig. 12 Integrated transfer functions in the two apertures

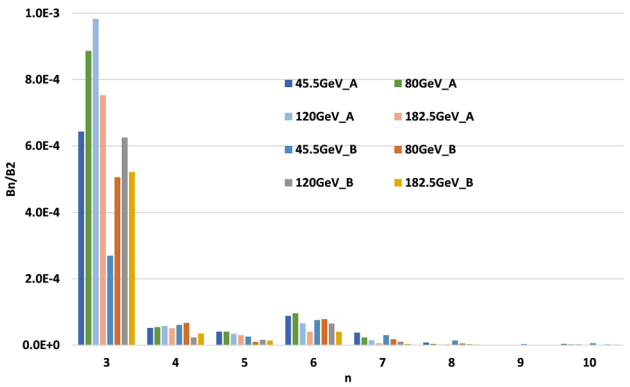

Fig. 13 (Color online) Measured field harmonics at different energies in two apertures of DAQ magnet

With increasing current, the difference decreased, i.e., to less than 0.1% at 234 A.

The measured normal and skew multipole field errors for the two apertures at different currents are presented in Fig. 13. The field harmonics were less than 1×10^{-4}, except for the sextupole component. The sextupole component is the first nonsystematic harmonic of the quadrupole magnet and is easily affected by pole profile errors, gap height deviations, and magnet assembly errors. The magnetic center is approximately 0.5 mm in the two apertures, and the magnetic center shift in the energy range is approximately 0.1 mm in aperture A and 0.075 mm in aperture B.

5.2 Magnetic center reduction

As mentioned in Sect. 3, the field crosstalk effect introduces large b_1 components in both apertures. In the modification of the DAQ magnet prototype, the center-protruding shim was 70 mm wide and 41 mm high, and the gap height between the yoke centers was 24 mm. The second modification involved reducing the upward and downward shim blocks by 1 mm, with the gap height between the center yokes of 26 mm.

The field was measured after adjusting the center gap height to 26 mm, and the results are listed in Table 3. At Higgs mode, the magnetic center in the *X*-direction reduced from 0.51 to 0.162 mm in aperture A and from 0.505 to 0.177 mm in aperture B; the corresponding variations are 0.348 and 0.328 mm. Normal sextupole component b_3 increased by 22.9 and 25.4 units in apertures A and B, respectively. The change in the magnetic center in the *Y*-direction was very small, and the skew sextupole component in the two apertures remained almost unchanged. It can be seen that the variation of b_3 in the two apertures is basically the same, indicating that the adjustment of the intermediate pad at the middle of the two apertures is mostly symmetrical, which is consistent with the simulation results. The change in the ratio of b_3 to b_1 was still around 0.08.

5.3 Harmonics compensation

A harmonics compensation method based on magic fingers was employed to reduce the field harmonics, as described in detail in this section. We replaced the old copper plates with stainless steel plates, as depicted in Fig. 14. These plates were used to ensure the rigidity of the pole and reduce lifting deformation.

Magic finger adjustment technology is employed to compensate for high-order nonsystematic harmonics, such as the sextupole and octupole components in quadrupole magnets [31]. The magic finger is made of pure solid iron (DT4) and has a slender rectangular shape, 11 mm wide, 8 mm thick, and 38 mm radial length. It fits in the slot in the connecting plates at different angles and positions, with its centerline passing through the center of the aperture. The magic finger was tightly attached to the pole using screws. The designated multipole magnetic field was generated by the symmetric and periodic arrangement of several fingers to cancel out the existing magnetic field harmonics. When the quadrupole magnet is energized, the magic finger installed at the pole is magnetized and generates a magnetic field that acts as a local current

Table 3 Magnetic center in mm and sextupole component units of 1×10^{-4} in DAQ before and after changing the center shim @120 GeV

	x_0_A	y_0_A	b_3_A	a_3_A	x_0_B	y_0_B	b_3_B	a_3_B
Before	0.510	0.133	− 9.30	− 3.19	− 0.505	− 0.070	− 6.17	− 1.0
After	0.162	0.131	13.60	− 3.74	− 0.177	− 0.061	19.2	− 0.98
Change	− 0.348	− 0.002	22.9	0.55	− 0.328	0.009	25.40	− 0.02

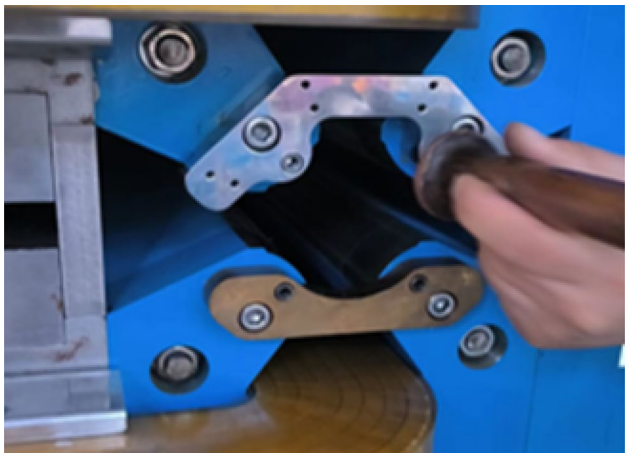

Fig. 14 (Color online) Connecting plate replacement. Top is the new stainless steel plate with finger slots; Bottom is the old copper plate

source. A magic finger generates various high-order components including normal and skewed terms. The proportions of the normal and skewed components differed according to the finger angle. As the harmonic order increases, the harmonic amplitude decreases. For a quadrupole magnet, the largest multipole field is typically the sextupole component.

There is one upper and one bottom connecting plate in each aperture at each end of the magnet. One plate constitutes four magic finger slots, as shown in Fig. 15, totally 16 magic finger slots at both ends in one aperture, at the angles of π/8, 3π/8, 5π/8, 7π/8, 9π/8, 11π/8, 13π/8, and 15π/8. With multipole fingers, the total harmonics are the algebraic sums of the magnetic fields generated by each magic finger.

Specific harmonics can be produced when the magic fingers are combined at different angles. The desired higher-order field was obtained through symmetry field cancelation and finger enhancement at different angles. For canceling the normal sextupole component, two fingers were predominantly used at angles of 5π/8 and 11π/8, which will generate larger b_3 and lower negative b_1, but without skewing the components of a_1 and a_3. The amplitude of the field multipole is determined by the size, material of the magic finger, and the radial distance of the magic finger to the aperture center of the quadrupole magnet. The nearer the magic finger is to the aperture center, the larger the generated magnetic field harmonics. As an auxiliary method, the adjustment ability of the magic fingers is limited.

As shown in Table 3, there are large b_3 components and certain a_3 components in aperture A. Figure 16 presents the layout of the magic fingers in aperture A (five magic fingers on the left), where magic fingers 1–4 are used to adjust the b_3 component, and magic finger 5 is used to adjust the a_3 component. In aperture B, there are four symmetrical magic fingers distributed in the same way as in aperture A, but without the finger at 15π/8 (location 5) because there is a very small skew sextupole component in aperture B.

The b_3 component changed from a positive to a negative value when the current was increased, and the variation was approximately five units, as detailed in Table 4. The final measured field harmonics after harmonic compensation are shown in Fig. 17. All the harmonics are less than five units, which meets the requirements.

In the four energy ranges, the magnetic center in the *X*-axis varies by 0.07 mm in aperture A and 0.131 mm in aperture B. The offset of the magnetic center in the *X*-direction was almost the same when the gap between the upper and lower shim centers was 24 and 26 mm. This offset may have been caused by the magnetic hysteresis. The magnetic center in the *Y*-direction varied by 0.029 mm for aperture A and only 0.006 mm for aperture B. Because the collider runs at one energy level each time for several years, and the interval between the four energies is long, the fixed offset of

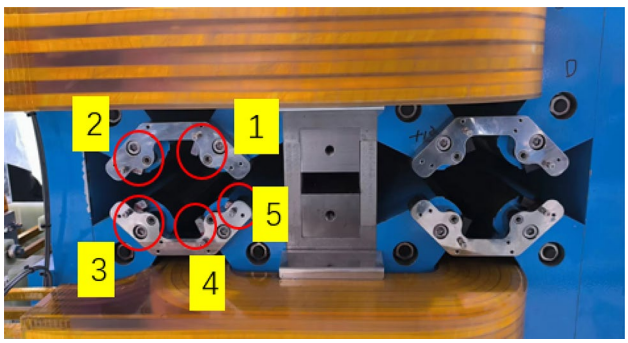

Fig. 16 (Color online) Magic fingers in the two apertures

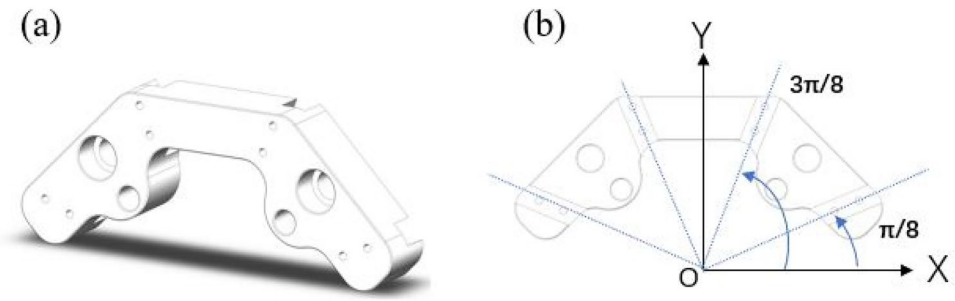

Fig. 15 (a) 3D model and (b) back view of connecting plates with magic finger slots

Table 4 Measured magnetic centers in mm and field harmonics in units of 1×10^{-4} at four currents

E (GeV)	x0_A	y0_A	b_3_A	a_3_A	x0_B	y0_B	b_3_B	a_3_B
45.5	− 0.082	0.084	2.46	− 4.24	0.044	− 0.007	3.64	− 0.83
80	− 0.039	0.081	− 1.20	− 3.76	− 0.018	− 0.009	− 3.04	− 1.18
120	− 0.021	0.075	− 2.2	− 3.15	− 0.054	− 0.012	− 1.52	− 1.52
180	− 0.012	0.055	1.94	− 1.92	− 0.087	− 0.007	1.98	− 0.79

the magnetic center in the X-axis can be corrected using trim coils or dipole magnets. Thus, the magnetic center shift can be accepted in accelerator physics.

6 Summary

A DAQ magnet is a key component of the CEPC ring. However, the main challenges include the field crosstalk between the two apertures, field adjustability with trim coils, and suppression of the magnetic center shift in the beam energy range.

Accordingly, a novel method was proposed to compensate for the crosstalk effect using a center shim to adjust the flux distribution in the iron in one aperture. As a result, the entire iron yoke scheme was selected as the baseline for the DAQ magnet and used to reconstruct the prototype. A separate iron core scheme was suggested as an alternative. Different layouts of the trim coils were simulated and compared. Then, the scheme of trim coils at the pole position was chosen, which has a minimum and balanced reluctance between the four poles in a single aperture with almost no effect on the field quality in another aperture. Because the relationship between the dipole and sextupole components varies in the 2D and 3D models, the final optimization should be based on 3D simulations. After the optimization and modification of the short quadrupole magnet prototype, the field performance met the requirements.

The development of the short DAQ magnet prototype at CEPC provides a reference for the optimization design and further development of DAQ magnets in various colliders.

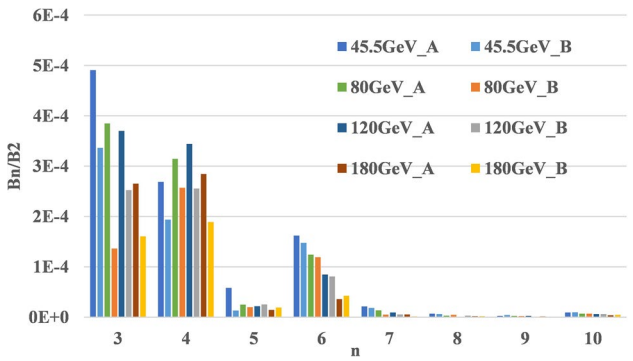

Fig. 17 (Color online) Higher order harmonics in two apertures at four different energies

Acknowledgements The authors would like to thank Yi-Wei Wang for technical discussions and for providing useful information about physics. Special thanks go to colleagues at Beijing HE-Racing Technology Co., Ltd., for their invaluable support in magnet manufacture and modification.

Author contributions All authors contributed to the study conception and design. The modeling, simulation, discussion, material preparation, and analysis of DAQ were performed by Mei Yang and Fu-San Chen. The field measurement and data collection were performed by Ya-Feng Wu, Zhuo Zhang, and Bao-Gui Yin. The mechanical design, mechanical analysis, and machining process of DAQ were performed by Bin Na and Zhan-Jun Zhang. The first draft of the manuscript was written by Mei Yang, and all authors commented on previous versions of the manuscript. All authors read and approved the final manuscript.

Data availability The data that support the findings of this study are openly available in Science Data Bank at https://doi.org/10.57760/sciencedb.j00186.00103 and https://cstr.cn/31253.11.sciencedb.j00186.00103.

Declarations

Conflict of interest The authors declare that they have no competing interests.

References

1. The CEPC Study Group, CEPC conceptual design report volume i-accelerator, IHEP-CEPC-DR-2018-01, IHEP-AC-2018-01 (2018). https://doi.org/10.48550/arXiv.1809.00285
2. J. Gao, S. Jin, Review of electron-positron colliders at the high-energy frontier (in Chinese). Chin. Sci. Bull **60**, 1251–1260 (2015). https://doi.org/10.1360/N972014-00820
3. J. Gao, Y.H. Li, J.Y. Zhai et al., *Key Technologies of High Energy Particle Accelerator* (Shanghai Jiaotong University Press, Shanghai, China, 2021)
4. Y.W. Wang, X.H. Cui, J. Gao, A beam optics design of the interaction region for the CEPC single-ring scheme. Int. J. Mod. Phys. A **34**(10), 1940007 (2019). https://doi.org/10.1142/S0217751X19400074
5. European Organization for Nuclear Research, LEP design report: Vol II the LEP main ring. CERN-LEP/84-01, (1984)
6. BEPCII Group, Design report of BEPCII, (2002)
7. C. Zhang, BEPCII: construction and commissioning. Chinese Phys. C **33**, 60 (2009). https://doi.org/10.1088/1674-1137/33/S2/016
8. The FCC Collaboration, FCC-ee: the lepton collider: future circular collider conceptual design report volume 2. Eur. Phys. J. Special Top. **228**(2), 261–623 (2019). https://doi.org/10.1140/epjst/e2019-900045-4

9. A. Milanese, Efficient twin aperture magnets for the future circular e+/e- collider. Phys. Rev. Accel. Beams **19**(11), 112401 (2016). https://doi.org/10.1103/PhysRevAccelBeams.19.112401
10. I. Agapov, M. Benedikt, A. Blondel, et al., Future circular lepton collider FCC-ee: Overview and status (2016). arXiv: 2203.07804 [physics.acc-ph]
11. J.Y. Zhai, D.J. Gong, H.J. Zheng et al., Design of CEPC superconducting RF system. Int. J. Mod. Phys. A **34**(10), 1940006 (2019). https://doi.org/10.1142/S0217751X19400062
12. H.J. Zheng, J. Gao, J.Y. Zhai et al., RF design of 650-MHz 2-cell cavity for CEPC. Nucl. Sci. Tech. **30**, 155 (2019). https://doi.org/10.1007/s41365-019-0671-6
13. Y.W. Wang, F. Su, S. Bai et al., Lattice design for the CEPC double ring scheme. Int. J. Mod. Phys. A **33**(2), 184001 (2018). https://doi.org/10.1142/S0217751X18400018
14. Y.W. Wang, S. Bai, C.H. Yu et al., The energy sawtooth effects in the partial double ring scheme of CEPC. Int. J. Mod. Phys. A **34**, 1940008 (2019). https://doi.org/10.1142/S0217751X19400086
15. Z.S. Yin, Y.Z. Wu, J.F. Zhang et al., Design and field measurement of the BEPCII interaction region dual-aperture quadrupoles. Nucl. Instrum. Meth. A **573**(3), 323–328 (2007). https://doi.org/10.1016/j.nima.2006.12.029
16. Y.Z. Wu, C.H. Yu, F.S. Chen et al., The magnet system of the BEPCII interaction region. IEEE T. Appl. Supercon. **20**(3), 360–363 (2010). https://doi.org/10.1109/TASC.2010.2040027
17. M. Yang, F.S. Chen, X.J. Sun et al., Development of the CEPC collider prototype magnets. Int. J. Mod. Phys. A **36**(22), 2142009 (2021). https://doi.org/10.1142/S0217751X21420094
18. Opera simulation software, 2020, [Online]. Available: https://www.3ds.com/products-services/simulia/products/opera/. (Accessed on March 2020)
19. A. Milanese, J. Bauche, C. Petrone, Magnetic measurements of the first short models of twin aperture magnets for FCC-ee. IEEE T. Appl. Supercon. **30**(4), 1–5 (2020). https://doi.org/10.1109/TASC.2020.2976949
20. G. Le Bec, J. Chavanne, C. Benabderrahmane et al., High gradient quadrupoles for low emittance storage rings. Phys. Rev. Accel. Beams **19**(5), 052401 (2016). https://doi.org/10.1103/PhysRevAccelBeams.19.052401
21. M. Johansson, B. Anderberg, L.J. Lindgren, Magnet design for a low-emittance storage ring. J. Synchrotron Radiat. **21**(5), 884–903 (2014). https://doi.org/10.1103/PhysRevAccelBeams.19.052401
22. T. Zickler, Basic design and engineering of normal-conducting, iron-dominated electromagnets. CERN Accelerator School CAS 2009: Specialized Course on Magnets, Bruges, (2009). Doi: https://doi.org/10.5170/CERN-2010-004.65
23. Y.S. Zhu, M. Yang, F.S. Chen et al., Development of a high precision small aperture quadrupole magnet with copper plate coils. Nucl. Instrum. Meth. A **1013**, 165652 (2021). https://doi.org/10.1016/j.nima.2021.165652
24. J.J. Zhao, Z.S. Yin, *Particle Accelerator Technology* (Higher Education Press, Beijing, 2006)
25. M. Yang, F.S. Chen, B.G. Yin et al., A rotating coil measurement system based on CMM for high-gradient small-aperture quadrupole in HEPS-TF. Radiat. Detect. Tech. Methods **5**(1), 8–14 (2021). https://doi.org/10.1007/s41605-020-00211-y
26. J.T. Tanabe, *Iron Dominated Electromagnets: Design, Fabrication, Assembly and Measurements* (World Scientific Publishing Company, Singapore, 2005). https://doi.org/10.48550/arXiv.1103.1119
27. A.K. Jain, Harmonic Coils. CAS-Measurement and alignment of accelerator and detector magnets, Anacapri, Italy, (1997), CERN 98-05, P. 175
28. J.X. Zhou, L. Li, B.G. Yin et al., A harmonic coil measurement system based on a dynamic signal acquisition device. Nucl. Instrum. Meth. A **624**, 549–553 (2010). https://doi.org/10.1016/j.nima.2010.10.009
29. A.K. Jain, Measurements of field quality using harmonic coils. US Particle Accelerator School on Superconducting Accelerator Magnets, Houston, Texas, USA (2001)
30. Q.L. Peng, F.L. Ren, B.G. Yin et al., Rotating coil field measurement of superconducting magnet for BEPCII interaction region. Nucl. Instrum. Meth. A **640**(1), 13–18 (2011). https://doi.org/10.1016/j.nima.2011.03.015
31. Y.S. Zhu, F.S. Chen, L. Wu, China Patent, ZL 201710613136.3, (2019)